

SegICL: A Universal In-context Learning Framework for Enhanced Segmentation in Medical Imaging

Lingdong Shen^{1,2,3*}, Fangxin Shang³,
Yehui Yang^{3†}, Xiaoshuang Huang^{3*}, and Shiming Xiang^{1,2}

¹ School of Artificial Intelligence, University of Chinese Academy of Sciences

² MAIS, Institute of Automation, Chinese Academy of Sciences

³ Healthcare Group, Baidu Inc.

* Work performed during an internship at Baidu

† Corresponding author, yangyehuisw@126.com

Abstract. Medical image segmentation models adapting to new tasks in a training-free manner through in-context learning is an exciting advancement. Universal segmentation models aim to generalize across the diverse modality of medical images, yet their effectiveness often diminishes when applied to out-of-distribution (OOD) data modalities and tasks, requiring intricate fine-tuning of model for optimal performance. For addressing this challenge, we introduce SegICL, a novel approach leveraging In-Context Learning (ICL) for image segmentation. Unlike existing methods, SegICL has the capability to employ text-guided segmentation and conduct in-context learning with a small set of image-mask pairs, eliminating the need for training the model from scratch or fine-tuning for OOD tasks (including OOD modality and dataset). Extensive experimental validation of SegICL demonstrates a positive correlation between the number of prompt samples and segmentation performance on OOD modalities and tasks. This indicates that SegICL effectively address new segmentation tasks based on contextual information. Additionally, SegICL also exhibits comparable segmentation performance to mainstream models on OOD and in-distribution tasks. Our code will be released after paper review.

Keywords: Medical Image Segmentation · Large Multi-Modal Model · Train-free Zero/Few Shot Learning

1 Introduction

Medical image segmentation is a crucial component of biomedical image analysis and has become a vital tool in medical diagnosis and health monitoring. Medical image segmentation models have evolved from initial convolutional neural network (CNN) structures [8, 30, 48] to the current transformer architectures [6, 15, 35, 42]. Preliminary research outcomes have also been achieved in areas such as efficient data utilization [3, 24] and the design of universal models [5, 22, 26]. With the advancements in this area, the efficient utilization of

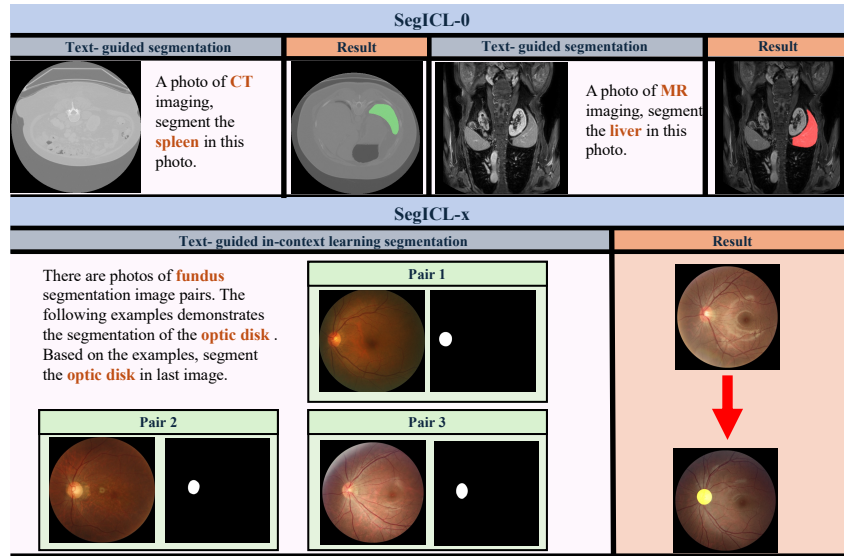


Fig. 1: The example of inference pipeline of SegICL. The upper part demonstrates SegICL can following text instructions. The lower part demonstrates SegICL can segment OOD data with a few image-mask pairs and text instructions.

models for high-quality, multi-modal, and learnable medical image segmentation has emerged as a research hotspot.

In medical image segmentation, two key research directions emerge: handling OOD tasks, and segmentation of regions of interest. Existing methods for the above two issues can be categorized into two types: specialized models designed for specific tasks and universal segmentation methods.

Firstly, specialized model for OOD tasks, like few-shot learning [17, 34, 39] paradigm aimed at improving the generalization of the model to new data with a small number of examples. Another approach involves enhancing the model’s generalization performance through data augmentation and pseudo-labels [3, 4, 23, 24, 36, 43, 45]. There are also universal segmentation models, designed to handle segmentation tasks across multiple medical modalities. However, specialized model’s generalization performance is mediocre, particularly when facing cross-modal or new tasks. While universal segmentation models exhibit good generalization performance, they are unable to handle OOD tasks. However, given the rapid progress in the medical field, if a completely new modality of medical imaging is utilized, all the above models would require retraining or fine-tuning.

Secondly, for segmentation of regions of interest, one of the existing solutions is to build a universal segmentation model based on SAM [19]. It utilizes geometric information such as points and boxes as prompts to guide the model in segmentation. Consider an interesting question: How can an annotator lacking

professional medical training quickly annotate organs they are unfamiliar with on medical images they don't understand? For instance, given a CT imaging, how can an annotator who lacks knowledge about the shape and approximate location of the 'spleen' quickly annotate its position?

As illustrated in Fig. 1, SegICL tackles these two issues through a text-guided interactive in-context learning paradigm. Unlike existing specialized model and universal segmentation model that demand retrain or fine-tuning to improve the segmentation performance on OOD tasks, SegICL is a train-free method which segments regions of interest by integrating text instructions and a few image-mask pairs. By leveraging a few number of image-mask pairs, SegICL achieves remarkable performance improvement on OOD tasks.

In summary, our contributions are as follows:

- For the first time, we propose a universal in-context learning paradigm for medical image segmentation. In this learning paradigm, the model can learn an in-context visual representation and follow text instructions.
- SegICL utilizes in-context learning to solve segmentation of OOD tasks issues, tackles region-of-interest segmentation through text instructions.
- Extensive experiments have demonstrated that SegICL exhibits impressive performance across multiple medical image segmentation datasets, showcasing competitive capabilities comparable to other SOTA methods.

2 Related work

2.1 Universal Medical Image Segmentation

With the rise of universal vision models such as CLIP [28], SAM [20] and SegGPT [38], the field of biomedical image segmentation has also witnessed a surge in research on universal medical segmentation models.

These studies can be classified into two types. One type involves fine-tuning or replacing new modules based on existing general vision models (such as SAM) [7, 9, 22, 40, 46]. For example, SAMed [46] adopts a low-rank-based fine-tuning strategy (LoRA) on top of SAM, fine-tuning the SAM image encoder on labeled medical image segmentation datasets. Another example is Med-SA [40], which differs from fine-tuning the SAM model by proposing the Medical SAM Adapter (Med-SA), incorporating domain-specific medical knowledge into the segmentation model. The other type involves training specialized universal medical segmentation models from scratch based on large-scale datasets. For instance, UniverSeg [5] utilizes a novel CrossBlock mechanism to generate accurate segmentation maps without requiring additional training, achieving generalization to new tasks.

Our approach differs from the methods mentioned above. The core of our proposed paradigm lies in a multi-modal input-driven segmentation method that incorporates in-context learning based on textual instructions. None of the aforementioned methods can simultaneously achieve both text-guided segmentation and context-aware segmentation, which are the two core aspects of our approach.

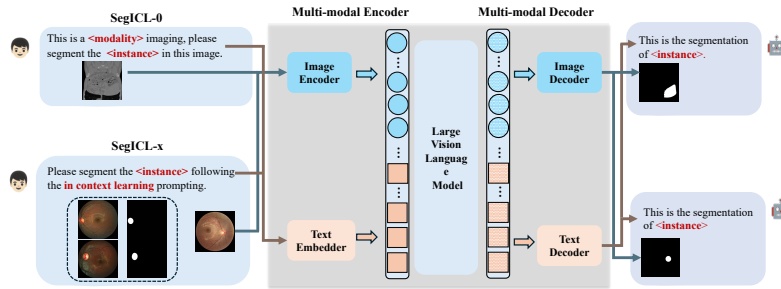


Fig. 2: The overall structure of the SegICL paradigm. SegICL-0 represents zero-shot inference, while SegICL-x represents using x image-mask pairs as prompts for inference.

2.2 Learning from limited data samples

Few-shot medical image segmentation [2, 17, 33, 34, 37, 39] is designed to efficiently address the scarcity of learning and generalizing from a limited number of samples. In the context of segmentation tasks, few-shot learning is introduced to segment unseen classes with the support of a limited amount of labeled data.

VQNet [45] introduces a VQ learning mechanism with Grid-Format VQ (GFVQ), Self-Organizing VQ (SOVQ), and Residual-Guided VQ (ROVQ) to medical MR imaging segmentation. SE-Net [31] incorporate few-shot learning for segmenting abdominal organs in CT images. RPNet [34] proposed a method that involves a context relation encoder (CRE) for capturing local relation features and a recurrent mask refinement module. This module iteratively refines the segmentation mask by utilizing the CRE and a prototypical network.

SegICL’s motivation aligns with few-shot learning, aiming to learn OOD tasks or adapt to OOD datasets or modality with minimal annotated data. However, unlike the aforementioned methods, these approaches exhibit poorer generalization performance, making them challenging to apply across modalities and tasks. Moreover, when confronted with OOD tasks from different modalities, they struggle to segment without the need for retraining. In contrast, the proposed paradigm possesses the capability of multi-modal context learning, enabling it to achieve learning without retraining when facing OOD tasks.

3 Methodology

3.1 Learning Paradigm of SegICL

The learning paradigm of SegICL aims to utilize information from multi-modal input, enabling the model to model and extract implicit data correlations in multi-modal data. Additionally, it empowers the model with the ability to perform segmentation using text-guided methods.

$$H = Enc(X_{img}, X_{text}) \quad (1)$$

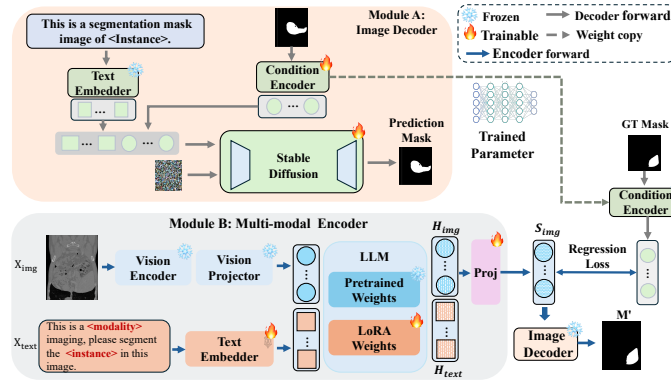


Fig. 3: Training pipeline of SegICL. Module A is a image decoder (Dec_{img}), and Module B is a Multi-modal encoder (Enc). Interleaved multi-modal text and image input undergoes encoding in Module B (get the hidden variable H_{img}), and the projected features (S_{img}) is then passed to Module A for decoding, ultimately generating the corresponding mask (M').

$$S_{img} = Proj(H_{img}) \quad (2)$$

The learning paradigm of SegICL (See Fig. 2) can be represented as Eqs. (1) to (3): where X_{img} and X_{text} represents the input including images and texts respectively, Enc is a large vision language model. After passing the multi-modal input through Enc , it obtains a hidden variable (H). Then, using a projector to align the H of the encoder with the feature space of the decoder, obtaining the encoded result state (S). Finally, the state is fed into the Dec_{img} for decoding, resulting in the final output mask.

$$M' = Dec_{img}(S_{img}) \quad (3)$$

The Enc is a trainable function that accepts multi-modal input and regresses to a hidden state features. The Dec can be any image generation model, decoding the final prediction from above state. The Enc 's supervision signal comes from the regression loss between the encoded result state and the condition encoder (See Fig. 3). The Dec_{img} 's supervision signal comes from the regression loss between the generated image and the ground truth masks.

3.2 SegICL

Building upon the aforementioned learning paradigm, to our best knowledge, SegICL is the first text-guidance in-context learning framework for medical image segmentation.

This framework (See Fig. 3) use a LLM implementing the Enc to model the input multi-modal data. Additionally, it includes a diffusion model (Dec_{img}) to

decode the state vector outputted by the encoder, yielding the final prediction. A 4-layer Multi-Layer Perceptron (MLP) serves as the shared condition encoder to provide regression targets for the encoder model.

$$M' = Dec_{img}(Proj((Enc(X_{img}, X_{text})))) \quad (4)$$

The forward computation of the framework is represented by the equation above (see Eq. (4)). This framework initially takes arbitrary interleaved textual and visual data as input. After processing through a visual encoder and a text encoder, it generates interleaved tokens of text and image (See Fig. 3 module B). These tokens serve as input for the multi-modal model, generating latent variables within a transformer structure rich in causal self-attention mechanisms.

Since the encoder and decoder are decoupled, a projector is needed to map the model’s feature space. After the tokens pass through the projector, a state vector is generated and made available for the decoder. The decoder model utilizes a diffusion model to ensure the quality of the generated images. When the input state vector is provided to the decoder model, it introduces random noise and uses the state vector as a condition to predict the output mask (See Fig. 3 module A).

SegICL’s diffusion decoder is trained using a substantial amount of ground truth mask images. Its input includes random noise and a conditional vector (obtained by encoding mask images through the condition encoder). The output is a mask image, with the goal of reconstructing the original image using the vector provided by the shared condition encoder.

3.3 Multi-modal Encoder

In contrast to existing multi-modal large models [1, 2, 12, 33], the multi-modal encoder used in this paper aims to regress the supervision signals provided by the condition encoder. Therefore, in the model design, a lightweight condition encoder is incorporated for supervised fine-tuning of the multi-modal large model.

Multi-modal encoder’s network architecture of the encoder is depicted in Fig. 2 module A. The visual encoder utilize CLIP ViT-big-G [28] as the base model and added a single-layer randomly initialized cross-attention layer on it. Visual encoder trained with 1.5 billion text-image data, the model supports an input image resolution of 448×448 , significantly enhancing its performance for fine-grained segmentation tasks. The language base model uses the pre-trained Qwen-7B model, contributing to a substantial reduction in the difficulty of transfer training, thanks to this excellent open-source work.

$$\mathcal{L} = \frac{1}{n} \sum_{i=1}^n (S_i - \hat{C}_i)^2 \quad (5)$$

The condition encoder implemented with a same 4-layer MLP structure as the diffusion’s condition encoder, ensures a lightweight network architecture to maintain model performance while significantly simplifying training complexity and parameter volume. We have standardized the input length for images,

encoding each image into 256 tokens. Consequently, the language model’s final output is a token sequence with this length. Inspired by LLaVA, we employed a simple projection layer to transform the feature space from the language model to the same feature space as the condition encoder. Ground truth masks have already undergone encoding by the condition encoder, producing a conditional variable with a length of 256. By infinitely narrowing the gap between the output of the teacher network and the output of the language model, we can ensure the final generation quality of the decoder. Therefore, the loss function for the multi-modal encoder is as shown above Eq. (5), using the MSE loss function to efficiently model the latent mapping between result state S_i and \hat{C}_i , where S_i represent projected image token, \hat{C}_i represent the ground truth masks encoded by condition encoder.

In addition, the exploration involves utilizing CLIP-ViT-big-G as the condition encoder and fitting multi-modal encoder’s output with its output. Experimental comparisons will be presented in the appendix to elucidate our choice.

3.4 Image Decoder

The image decoder can be any model capable of performing image generation tasks. In this paper, ControlNet [47] is chosen as the image decoder, and its model structure can be referred to in Fig. 3, Module B. In this context, the task of the image decoder is to accept a set of conditional vectors and generate images based on these vectors.

$$\mathcal{L} = \mathbb{E}_{m_0, t, c_k, c_t, \epsilon \sim \mathcal{N}(0,1)} \left[\|\epsilon - \epsilon_\theta(m_t, t, c_k, c_t)\|_2^2 \right] \quad (6)$$

We utilized the pre-training parameters of the Stable Diffusion 1.5B [29] model to ensure the image decoder could be trained with relatively less data while achieving excellent image generation results. The training process for the image decoder can be conceptualized as the recovery of input image features from the conditioned vectors. Initially, the input image is fed into the designated conditional encoder, extracting features from the input image to generate conditional variables. Subsequently, the conditional variables are injected into the backbone network using cross-attention. The loss is calculated by comparing the noise to optimize the entire image encoder during the training process (See Eq. (6)). A mask image as input (m_0), then diffusion algorithms progressively introduce noise to the image, generating a noisy image (m_t). Subsequently, with the keyword prompt (c_k) and the feature vector output from the conditional model(c_t) as auxiliary, a function (ϵ_θ) is employed to predict noise.

4 Experiments

To validate the effectiveness of our work, we chose three modalities and conducted a comprehensive evaluation of our approach on five datasets. Experimental results demonstrate that SegICL exhibits outstanding in-context learning capabilities and delivers competitive results across multiple datasets.

4.1 Dataset

71 publicly available datasets is utilized as the training set, referred to as the in-distribution datasets (details can be found in the supplementary materials).

Additionally, we reserved the fundus segmentation task to evaluate SegICL’s learning capabilities for OOD tasks. Furthermore, for each modality, we retained some datasets to assess the performance of SegICL on OOD tasks. Regarding the training set, we preserved a portion as the test set for evaluating the model’s segmentation performance on in-distribution data.

The evaluation perform on three fundus datasets, along with one CT dataset and one MR dataset. Additionally, we applied the approach described in [44] to uniformly preprocess the experimental datasets.

REFUGE2 [14]. This dataset contains 2000 color fundus images with annotations of glaucoma classification, optic disc/cup segmentation, as well as fovea localization. We conducted evaluations on the optic disc/cup segmentation task.

PALM [13]. This dataset consists of 1200 images with labels for pathologic myopia, including manual annotations for the optic disc, fovea position. We chose evaluations on the optic disc segmentation task.

IDRiD [27]. This dataset includes disease severity information for diabetic retinopathy and diabetic macular edema in each image. There are five segmentation tasks, and we chose optic disc segmentation for the evaluation experiment.

CHAOS [18]. This dataset includes abdomen MRI data, which sourced from ISBI 2019 Combined Healthy Abdominal Organ Segmentation Challenge (Task 5). We focus on four segmentation classes: liver, left kidney, right kidney, spleen.

BTCV [21]. This dataset includes a total of 50 abdominal CT scans, obtained from patients with metastatic liver cancer or postoperative abdominal hernia. It involves 13 segmentation categories, and we adhere to the aforementioned evaluation metrics, focusing specifically on four segmentation classes: liver, left kidney, right kidney and spleen.

4.2 Implementation details

SegICL utilizes QWen-7B as the multi-modal encoder and ControlNet as the image decoder. A 4-layer MLP (Multi-Layer Perceptron) is used as both the condition encoder and the teacher module, with shared parameters between them. After the completion of training in the first stage, the parameters of condition encoder and the teacher module are frozen.

In the first stage, the image decoder is trained using 2M image mask data, and after training, all parameters of the image decoder are frozen. In the second stage, a two-stage instruction dataset is employed to train the multi-modal encoder, covering a total of 71 datasets, including 5 modalities, with a total of 200K instruction data. LoRA [16] fine-tuning is applied to the multi-modal encoder, while Full-parameter finetuning is employed for the projector part.

The Dice [10] score is used as the evaluation metric for the model. For the calculation of few-shot performance, we randomly sample data from the training set of the dataset under evaluation as example data. The final result is obtained

by averaging the pixel-wise results of 5 independently randomly sampled predictions, followed by post-processing through binarization of the output masks.

4.3 Performance of the OOD modality

This section primarily analyzes modalities and their segmentation tasks beyond the distribution of the training dataset. The fundus image data did not utilized in the training dataset for SegICL.

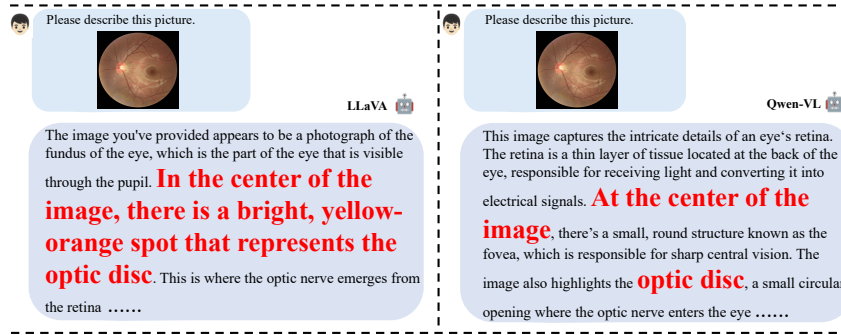


Fig. 4: Diagram of the differences between different base models. Different base models possess varying degrees of prior knowledge. Thanks to pre-trained weights, the model can roughly localize the target even in a zero-shot scenario.

Through experiments, it is found that multimodal large models naturally understand fundus images as shown in Fig. 4, and they can know the approximate shape and position of the optic disc. Therefore, different base models may lead to different performance changes, which is also a future direction of our work. Notably, our attained generalization capability is achieved without additional training and demands only a handful of relevant examples for substantial performance improvement.

We evaluated the effectiveness of SegICL on three datasets. (See Fig. 5) On the REFUGE2 dataset, employing SegICL-0 segmentation by directly using text prompts for optic disc and cup segmentation tasks resulted in scores of 0.447 and 0.294, respectively. This indicates that OOD tasks pose a challenging endeavor, requiring models to perform segmentation tasks effectively even in the absence of examples.

For the optic and disc segmentation task, introducing SegICL-1 lead to a performance improvement of 0.245, using SegICL-2 further increased performance by 0.059, and providing SegICL-2 resulted in an additional performance improvement of 0.088. It can be observed that with the addition of examples, SegICL can effectively capture the feature correlations between contexts, thereby transitioning OOD tasks from being undoable (poor performance) to achievable albeit with suboptimal performance.

Regarding the optic cup task, introducing SegICL-1 lead to performance improvements of 0.177, using SegICL-2 increased performance by 0.122, and providing SegICL-3 lead to a performance improvement of 0.079. On the PALM dataset, a similar trend is observed, with the Dice score increasing from 0.385 in SegICL-0 to 0.816 in SegICL-3, indicating that as the number of examples increases, the model gradually adapts to new segmentation tasks. On the IDRiD dataset, as the number of examples increased, the performance also gradually improved, with increments of 0.218, 0.093, and 0.084, respectively.

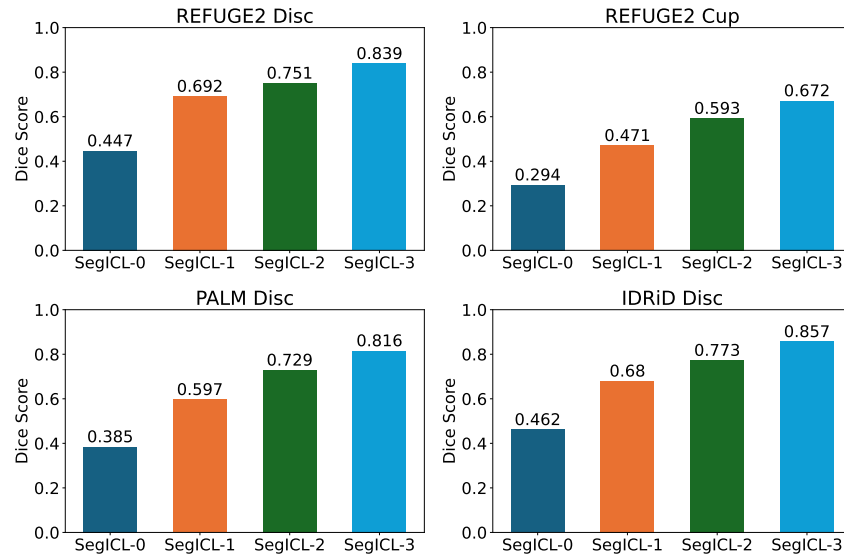


Fig. 5: Performance comparison of SegICL on OOD modality. The positive correlation can be observed between the number of prompt samples (SegICL-x) and segmentation performance. Although SegICL-3 doesn't match the SOTA models, its train-free results are still adequate for assisting cold-start in semi-automatic annotation.

Based on the above experiments, it can be concluded that SegICL possesses powerful in-context learning capabilities. When confronted with a new task without prior training, the segmentation performance is initially low. However, through example-based teaching, the model can grasp the segmentation approach for the task (See Fig. 6). With more examples provided for teaching, the model's segmentation performance on that task shows a linear growth. Furthermore, the observed performance enhancement exhibits a positive correlation with the number of examples provided (See Fig. 6 SegICL-0 to SegICL-3).

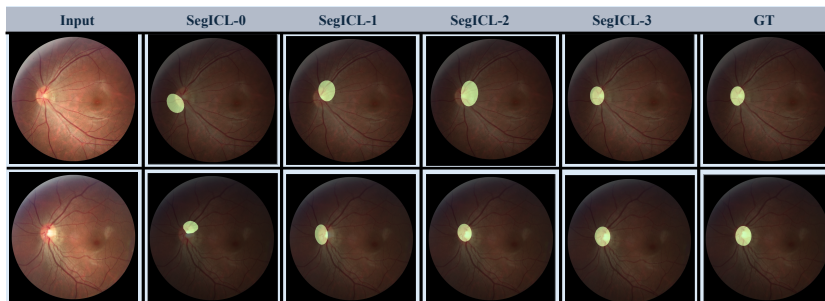


Fig. 6: The qualitative analysis diagram of SegICL on fundus segmentation tasks. As more examples are provided, the shape and position of the masks increasingly approximate the ground truth.

4.4 Performance of the OOD dataset

The generalization performance of SegICL is evaluated using an abdominal MR image dataset that did not appear in the training dataset. However, despite the presence of segmentation task data similar to the training dataset in this OOD dataset, they are not sampled from the same data distribution.

Method	Paradigm	Liver	Spleen	L.Kidney	R.Kidney	Mean
PANet [37]	1-shot	50.40	40.58	32.19	30.99	38.53
SE-Net [31]	1-shot	29.02	47.30	47.96	45.78	42.51
ALPNet [25]	1-shot	62.35	61.32	60.81	58.83	63.17
RPNNet [34]	1-shot	73.51	69.85	70.00	70.48	79.26
GCN-DE [32]	1-shot	49.47	60.63	83.03	76.07	67.03
VQNet [17]	1-shot	81.72	79.08	68.94	60.03	72.44
CRAPNet [11]	1-shot	76.46	74.32	81.95	86.42	79.79
SSL-ALPNet [25]	1-shot	76.10	72.18	85.18	81.92	78.84
SSL-VQNet [17]	1-shot	79.92	77.21	91.56	89.54	84.56
SegICL	ICL-0	70.91	62.95	82.20	80.47	73.95
	ICL-1	75.42	71.95	86.22	85.90	79.65
	ICL-3	79.47	78.92	92.18	89.95	85.13

Table 1: Performance comparison of SegICL and SOTA few-shot models on MRI dataset, SSL represents the utilization of self-supervised learning to enhance model performance, while SegICL-x stands for the number of samples for in-context learning.

In Tab. 1, we compared the performance of SegICL with SOTA few-shot methods. All few-shot methods are based on 1-way 1-shot settings. As shown in the table, our approach achieved an average Dice score higher than VQNet, by 1.52% in the SegICL-0 setting. Specifically, our SegICL-0 outperformed VQNet by 13.26% and 20.44% in Kidney segmentation. Compared to incorporating Self-Supervised Learning (SSL), SegICL, with the introduction of In-Context Learn-

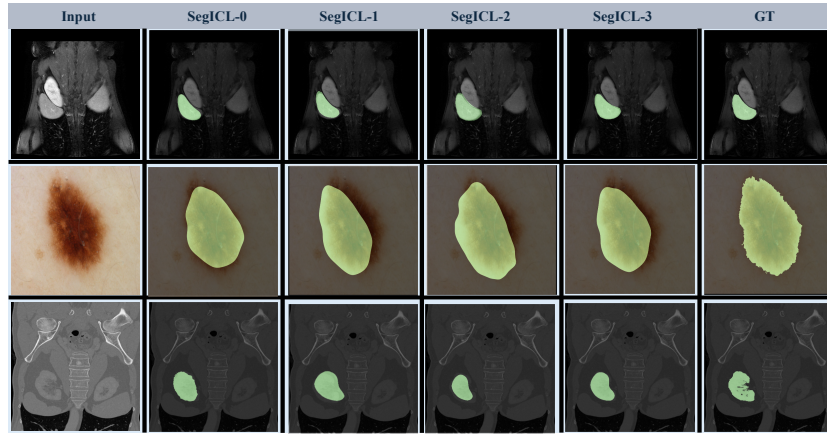


Fig. 7: The qualitative analysis diagram of SegICL on OOD dataset. Demonstrates that with an increase in provided examples, segmentation performance also improves.

ing (ICL), demonstrated further improvement in performance. Its average Dice score surpassed the strongest few-shot method, VQNeTs, by 0.57%. Moreover, it reached SOTA levels in spleen, left kidney, and right kidney sub-segmentation tasks. It is important to note that our method achieved inference in a completely train-free manner, avoiding the need to retrain the network with an SSL module. Additionally, the table reflects the necessity of In-Context Learning for performance enhancement on OOD tasks. It is evident that, for the four sub-classification tasks, performance improved by 8.56%, 15.97%, 9.98%, and 9.48%, respectively, resulting in an average Dice improvement of 11.18%. Thus, SegICL demonstrates robust generalization performance, achieving competitive results on OOD tasks with the incorporation of In-Context Learning.

SegICL demonstrates a certain level of generalization ability for OOD datasets and segmentation tasks. Moreover, as the number of example data increases, SegICL exhibits a capacity for learning new knowledge, with performance improving proportionally to the increase in example data.

From Fig. 7, it can be observed that the segmentation accuracy of SegICL improves with the increasing context information. The segmentation images of three different modalities are displayed, indicating that the model’s contextual learning ability is effective across various modalities.

4.5 Performance of the In-distribution datasets

In this section, we conducted performance evaluation of SegICL using the test set from the dataset that is previously used in the training set. As shown in Fig. 8, SegICL exhibits comparable performance to models trained specifically on dedicated datasets. We used nnU-Net, trained on the BTCV dataset through supervised learning, as the upper performance limit. In SegICL-0 inference, SegICL’s

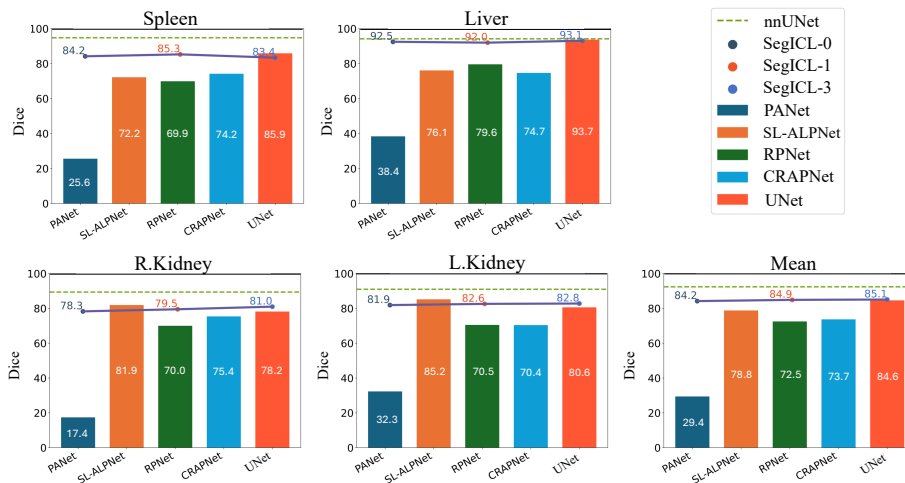


Fig. 8: Performance comparison on CT dataset. The performance of SegICL is comparable to that of models tailored specifically for this dataset.

performance differs from UNet by only 0.4%. After employing in-context learning with example data selected from the training set, our method’s average performance surpasses UNet by 0.5%, demonstrating the learning capability of SegICL.

Simultaneously, the table indicates that in this experimental setup, the learning capacity of SegICL is noteworthy. Through in-context learning, the model is able to capture contextual features of the segmentation task, leading to improved segmentation performance.

SegICL falls short of surpassing proprietary models trained specifically for dedicated datasets due to its training dataset encompassing multiple modalities from various datasets. As a result, its performance on a single dataset can only be competitive rather than achieving SOTA status. The primary purpose behind introducing SegICL is to propose a method capable of addressing OOD tasks through contextual learning with a limited number of examples. Achieving the utmost optimization in performance is a consideration for future work.

4.6 Qualitative results

For a more in-depth exploration of SegICL’s segmentation performance, we visualize four typical CT images featuring the liver, spleen, kidneys, and pancreas in Fig. 9. The results reveal that SegICL excels in segmenting CT slices with larger and more regular-shaped target volumes, such as the upper part displaying the liver and kidneys. However, its performance diminishes on CT slices with smaller and elongated target shapes. The segmentation edge localization capability is inadequate for all CT slices.

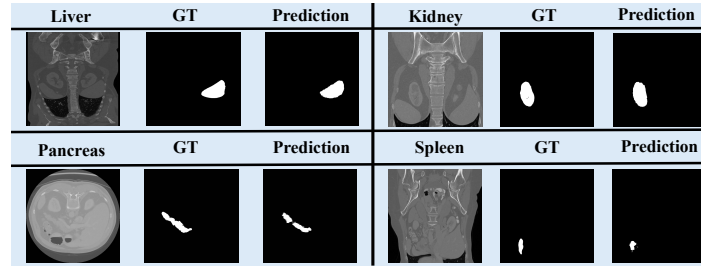


Fig. 9: Qualitative analysis results display: Segmentation results for different organs in CT imaging. Demonstrate the strengths and limitation of SegICL.

Qualitative analysis unveils two potential issues. Firstly, the limited modeling capacity of the multimodal encoder for the state vector. While larger models could enhance fitting, we opted for the 7B language model considering computation costs and model effectiveness. Secondly, the use of diffusion to generate segmentation masks inherits issues from the diffusion model, leading to a slight deficiency in generating fine-grained segmentation details. Nonetheless, existing medical segmentation works based on diffusion [41] have demonstrated its significant improvement in segmentation performance, maybe this issue can be solve. In summary, SegICL is a successful universal medical segmentation framework with robust context learning capabilities. The experiments confirm its efficacy. Future research will explore solutions to the aforementioned issues.

5 Discussion

This paper has several limitations: Firstly, due to our use of a pre-trained language model, the token length of inputs and outputs is limited by the settings of the base model, which prevents us from exploring the performance upper limit of SegICL-x. Secondly, there are issues with poor edge processing for the generated masks, even with post-processing, precise edge segmentation cannot be achieved. Therefore, it is necessary to explore new technologies to increase segmentation accuracy by increasing the token length and refining the mask edge.

Future research can be focused on the following three aspects: Firstly, training the model using larger models and datasets. Secondly, enhancing the quality of image generation and segmentation performance. From the above analysis (Sec. 4.6), it can be inferred that the segmentation performance of the model is related to the quality of image generation. Therefore, improving the details of generated images is also crucial for enhancing the performance of the model. Thirdly, accelerating the segmentation speed of the model. Due to the introduction of large language models and Diffusion models, the segmentation speed is relatively slow, so it is necessary to study how to improve the speed of the model.

6 Conclusion

In this study, we introduce SegICL, a pioneering approach to image segmentation leveraging text-guided segmentation and In-Context Learning (ICL) that effectively addresses the limitations of universal segmentation models on OOD task with a training-free manner. Our work paves the way for more intuitive, efficient, and effective segmentation models that can adapt to the rapidly evolving landscape of medical imaging.

References

1. Awadalla, A., Gao, I., Gardner, J., Hessel, J., Hanafy, Y., Zhu, W., Marathe, K., Bitton, Y., Gadre, S., Sagawa, S., et al.: Openflamingo: An open-source framework for training large autoregressive vision-language models. arXiv preprint arXiv:2308.01390 (2023)
2. Bai, J., Bai, S., Yang, S., Wang, S., Tan, S., Wang, P., Lin, J., Zhou, C., Zhou, J.: Qwen-vl: A versatile vision-language model for understanding, localization, text reading, and beyond (2023)
3. Bai, Y., Chen, D., Li, Q., Shen, W., Wang, Y.: Bidirectional copy-paste for semi-supervised medical image segmentation. In: CVPR. pp. 11514–11524 (2023)
4. Basak, H., Yin, Z.: Pseudo-label guided contrastive learning for semi-supervised medical image segmentation. In: CVPR. pp. 19786–19797 (2023)
5. Butoi, V.I., Ortiz, J.J.G., Ma, T., Sabuncu, M.R., Guttag, J.V., Dalca, A.V.: Universeg: Universal medical image segmentation. In: ICCV. pp. 21381–21394 (2023)
6. Chen, J., Lu, Y., Yu, Q., Luo, X., Adeli, E., Wang, Y., Lu, L., Yuille, A.L., Zhou, Y.: Transunet: Transformers make strong encoders for medical image segmentation. arXiv preprint arXiv:2102.04306 (2021)
7. Cheng, J., Ye, J., Deng, Z., Chen, J., Li, T., Wang, H., Su, Y., Huang, Z., Chen, J., Jiang, L., et al.: Sam-med2d. arXiv preprint arXiv:2308.16184 (2023)
8. Çiçek, Ö., Abdulkadir, A., Lienkamp, S.S., Brox, T., Ronneberger, O.: 3d u-net: Learning dense volumetric segmentation from sparse annotation. In: MICCAI. pp. 424–432 (2016)
9. Deng, R., Cui, C., Liu, Q., Yao, T., Remedios, L.W., Bao, S., Landman, B.A., Wheless, L.E., Coburn, L.A., Wilson, K.T., et al.: Segment anything model (sam) for digital pathology: Assess zero-shot segmentation on whole slide imaging. arXiv preprint arXiv:2304.04155 (2023)
10. Dice, L.R.: Measures of the amount of ecologic association between species. *Ecology* **26**(3), 297–302 (1945)
11. Ding, H., Sun, C., Tang, H., Cai, D., Yan, Y.: Few-shot medical image segmentation with cycle-resemblance attention. In: WACV. pp. 2487–2496 (2023)
12. Dong, R., Han, C., Peng, Y., Qi, Z., Ge, Z., Yang, J., Zhao, L., Sun, J., Zhou, H., Wei, H., et al.: Dreamllm: Synergistic multimodal comprehension and creation. arXiv preprint arXiv:2309.11499 (2023)
13. Fang, H., Li, F., Wu, J., Fu, H., Sun, X., Orlando, J.I., Bogunović, H., Zhang, X., Xu, Y.: Open fundus photograph dataset with pathologic myopia recognition and anatomical structure annotation. *Scientific Data* (1), 99 (2024)
14. Fang, H., Li, F., Wu, J., Fu, H., Sun, X., Son, J., Yu, S., Zhang, M., Yuan, C., Bian, C., et al.: Refuge2 challenge: A treasure trove for multi-dimension analysis and evaluation in glaucoma screening. arXiv preprint arXiv:2202.08994 (2022)
15. Gao, Y., Zhou, M., Metaxas, D.N.: Utinet: A hybrid transformer architecture for medical image segmentation. In: MICCAI. pp. 61–71 (2021)
16. Hu, E.J., Shen, Y., Wallis, P., Allen-Zhu, Z., Li, Y., Wang, S., Wang, L., Chen, W.: Lora: Low-rank adaptation of large language models. In: ICLR (2022)
17. Huang, S., Xu, T., Shen, N., Mu, F., Li, J.: Rethinking few-shot medical segmentation: A vector quantization view. In: CVPR. pp. 3072–3081 (2023)
18. Kavur, A.E., Gezer, N.S., Barış, M., Aslan, S., Conze, P.H., Groza, V., Pham, D.D., Chatterjee, S., Ernst, P., Özkan, S., et al.: Chaos challenge-combined (ctmr) healthy abdominal organ segmentation. *Medical Image Analysis* **69**, 101950 (2021)

19. Kirillov, A., Mintun, E., Ravi, N., Mao, H., Rolland, C., Gustafson, L., Xiao, T., Whitehead, S., Berg, A.C., Lo, W.Y., et al.: Segment anything. arXiv preprint arXiv:2304.02643 (2023)
20. Kirillov, A., Mintun, E., Ravi, N., Mao, H., Rolland, C., Gustafson, L., Xiao, T., Whitehead, S., Berg, A.C., Lo, W.Y., et al.: Segment anything. arXiv preprint arXiv:2304.02643 (2023)
21. Landman, B., Xu, Z., Igelsias, J., Styner, M., Langerak, T., Klein, A.: Miccai multi-atlas labeling beyond the cranial vault—workshop and challenge. In: Proc. MICCAI Multi-Atlas Labeling Beyond Cranial Vault—Workshop Challenge. vol. 5, p. 12 (2015)
22. Ma, J., He, Y., Li, F., Han, L., You, C., Wang, B.: Segment anything in medical images. *Nature Communications* **15**(1), 654 (2024)
23. Miao, J., Chen, C., Liu, F., Wei, H., Heng, P.: Caussl: Causality-inspired semi-supervised learning for medical image segmentation. In: ICCV. pp. 21369–21380 (2023)
24. Ouyang, C., Biffi, C., Chen, C., Kart, T., Qiu, H., Rueckert, D.: Self-supervision with superpixels: Training few-shot medical image segmentation without annotation. In: ECCV. pp. 762–780 (2020)
25. Ouyang, C., Biffi, C., Chen, C., Kart, T., Qiu, H., Rueckert, D.: Self-supervision with superpixels: Training few-shot medical image segmentation without annotation. In: ECCV. pp. 762–780 (2020)
26. Perslev, M., Dam, E.B., Pai, A., Igel, C.: One network to segment them all: A general, lightweight system for accurate 3d medical image segmentation. In: MICCAI. pp. 30–38 (2019)
27. Porwal, P., Pachade, S., Kamble, R., Kokare, M., Deshmukh, G., Sahasrabudhe, V., Meriaudeau, F.: Indian diabetic retinopathy image dataset (idrid): a database for diabetic retinopathy screening research. *Data* (3), 25 (2018)
28. Radford, A., Kim, J.W., Hallacy, C., Ramesh, A., Goh, G., Agarwal, S., Sastry, G., Askell, A., Mishkin, P., Clark, J., Krueger, G., Sutskever, I.: Learning transferable visual models from natural language supervision. In: ICML. pp. 8748–8763 (2021)
29. Rombach, R., Blattmann, A., Lorenz, D., Esser, P., Ommer, B.: High-resolution image synthesis with latent diffusion models. In: CVPR. pp. 10674–10685 (2022)
30. Ronneberger, O., Fischer, P., Brox, T.: U-net: Convolutional networks for biomedical image segmentation. In: MICCAI. pp. 234–241 (2015)
31. Roy, A.G., Siddiqui, S., Pölsterl, S., Navab, N., Wachinger, C.: ‘squeeze & excite’ guided few-shot segmentation of volumetric images. *Medical Image Anal.* **59** (2020)
32. Sun, L., Li, C., Ding, X., Huang, Y., Chen, Z., Wang, G., Yu, Y., Paisley, J.: Few-shot medical image segmentation using a global correlation network with discriminative embedding. *Computers in biology and medicine* **140**, 105067 (2022)
33. Sun, Q., Cui, Y., Zhang, X., Zhang, F., Yu, Q., Luo, Z., Wang, Y., Rao, Y., Liu, J., Huang, T., et al.: Generative multimodal models are in-context learners. arXiv preprint arXiv:2312.13286 (2023)
34. Tang, H., Liu, X., Sun, S., Yan, X., Xie, X.: Recurrent mask refinement for few-shot medical image segmentation. In: ICCV. pp. 3898–3908 (2021)
35. Valanarasu, J.M.J., Oza, P., Hacihaliloglu, I., Patel, V.M.: Medical transformer: Gated axial-attention for medical image segmentation. In: MICCAI. pp. 36–46 (2021)
36. Wang, H., Li, X.: Towards generic semi-supervised framework for volumetric medical image segmentation. In: NeurIPS (2023)
37. Wang, K., Liew, J.H., Zou, Y., Zhou, D., Feng, J.: Panet: Few-shot image semantic segmentation with prototype alignment. In: ICCV. pp. 9196–9205 (2019)

38. Wang, X., Zhang, X., Cao, Y., Wang, W., Shen, C., Huang, T.: Seggpt: Towards segmenting everything in context. In: ICCV. pp. 1130–1140 (2023)
39. Wu, H., Xiao, F., Liang, C.: Dual contrastive learning with anatomical auxiliary supervision for few-shot medical image segmentation. In: ECCV. pp. 417–434 (2022)
40. Wu, J., Fu, R., Fang, H., Liu, Y., Wang, Z., Xu, Y., Jin, Y., Arbel, T.: Medical sam adapter: Adapting segment anything model for medical image segmentation. arXiv preprint arXiv:2304.12620 (2023)
41. Wu, J., Fu, R., Fang, H., Zhang, Y., Xu, Y.: Medsegdiff-v2: Diffusion based medical image segmentation with transformer. arXiv preprint arXiv:2301.11798 (2023)
42. Yang, D., Myronenko, A., Wang, X., Xu, Z., Roth, H.R., Xu, D.: T-automl: Automated machine learning for lesion segmentation using transformers in 3d medical imaging. In: ICCV. pp. 3942–3954 (2021)
43. Yang, Z., Ren, M., Ding, K., Gerig, G., Wang, Y.: Keypoint-augmented self-supervised learning for medical image segmentation with limited annotation. In: NeurIPS (2023)
44. Ye, J., Cheng, J., Chen, J., Deng, Z., Li, T., Wang, H., Su, Y., Huang, Z., Chen, J., Jiang, L., et al.: Sa-med2d-20m dataset: Segment anything in 2d medical imaging with 20 million masks. arXiv preprint arXiv:2311.11969 (2023)
45. You, C., Dai, W., Min, Y., Liu, F., Clifton, D.A., Zhou, S.K., Staib, L.H., Duncan, J.S.: Rethinking semi-supervised medical image segmentation: A variance-reduction perspective. In: NeurIPS (2023)
46. Zhang, K., Liu, D.: Customized segment anything model for medical image segmentation. arXiv preprint arXiv:2304.13785 (2023)
47. Zhang, L., Rao, A., Agrawala, M.: Adding conditional control to text-to-image diffusion models. In: ICCV. pp. 3813–3824 (2023)
48. Zhou, Z., Rahman Siddiquee, M.M., Tajbakhsh, N., Liang, J.: Unet++: A nested u-net architecture for medical image segmentation. In: MICCAI. pp. 3–11. Springer (2018)